RASĀYAN *J. Chem.*
Vol. 19 | No. 1 | 114-122 | January-March | 2026
ISSN: 0974-1496 | e-ISSN: 0976-0083 | CODEN: RJCABP
http://www.rasayanjournal.com
http://www.rasayanjournal.co.in

SYNTHESIS AND DIELECTRIC PROPERTY EVALUATION OF COPPER OXIDE NANOSTRUCTURES, EVALUATING THEIR ELECTROCHEMICAL POTENTIAL FOR NOVEL SYMMETRIC SUPER CAPACITOR ELECTRODE APPLICATION

M. Sappani Muthu[1,✉], J. Judes[2], S. Arul Ravi[3], M. Ambrose RajKumar[4]
[1]Department of Electronics, St. Joseph's College (Autonomous) Tirchirappalli-620 002,Tamilnadu, India
[2]Department of Physics, Anna University Regional Campus, Tirunelveli-627 007, Tamilnadu, India,
[3]Department of Maths, St. Xavier's College (Autonomous), Palayamkottai-627 002, Tamilnadu, India
[4]Department of Physics, Kristu Jayanthi College (Autonomous), Bangaluru-560 077
✉Correspondance author: sappanimuthu_el2@mail.sjctni.edu

ABSTRACT
Polymorphic Copper oxide (CuO) nano-materials were synthesised by surfactant-assisted wet chemical and solid-state reaction methods. The effect of the surfactants (PVP, CTAB and Igepal 210) addition and heat treatment on structural, optical, dielectric and electrochemical properties of CuO nanomaterial was investigated and compared with the two preparation methods. A novel and cost-effective CuO electrode for a symmetric super capacitor was successfully prepared. The maximum specific capacitance of 747 Fg^{-1} at 5 $mVs^{-1}$was obtained for the CuO nanomaterial samples prepared using the solid state reaction method, and the competitive capacitance values were also observed for the CuO nanomaterial samples, synthesised via the wet chemical process with varied control parameters.
Keywords: XRD, W-H Plot, SEM, CV- Cyclic Voltammeter Studies, Dielectric Properties Studies.
RASĀYAN*J. Chem.*, Vol. 19, No.1, 2026

INTRODUCTION

In contemporary society, portability is widely valued across all sectors, and the market for portable devices is experiencing substantial growth. Portable electronic devices necessitate the advancement of portable energy storage solutions.[1,2] Recently, the concept of super capacitors has surpassed conventional energy storage devices based on electrochemical processes, excelling in power density, cycle life, rapid charge/discharge rates, compactness, reduced internal resistance, broader operational temperature ranges, and sustainable materials.[3.5] The super capacitor bridges the gap between the batteries and conventional capacitors. The electrochemical research sector is currently focused on the development of super capacitors with high capacitance and working voltage of cells. Super capacitor consists of two electrodes separated by ion-permeable separator immersed in an electrolyte. Each component plays a vital role in the performance of the super capacitor cell. More recently, experiments with carbon, metal oxide and conducting polymers have been conducted in super capacitor electrodes.[7-10] Transitional metal oxides are considered ideal electrode materials for pseudo capacitors because they provide variable oxidation states for efficient transfer of redox-charged energy.[11] CuO is a promising metal oxide due to its low cost, environmental friendliness, chemical stability, and non-toxicity.[12-14] Nonetheless, there has been limited research on the use of CuO for super capacitor electrodes due to its low electrical conductivity and inconsistent cycling performance.[15] The use of copper oxide electrodes in super capacitors was initially documented. Subsequent research on CuO super capacitors, particularly demonstrated that the morphology and synthesis process have a significant impact on the

http://doi.org/10.31788/RJC.2026.1919498

specific capacitance of CuO.[16] In this study, copper oxide nanostructures are prepared using both surfactant-assisted wet chemical technique and a solid-state reaction method. The effects of surfactant concentration and heat treatment on the synthesized CuO nanostructures have been thoroughly examined, focusing on their crystallite size, morphology and dielectric constant. The structural, optical, electrical, and photo catalytic characteristics of the synthesized CuO nanostructures are compared with earlier studies.[17] However; special emphasis is placed on assessing the dielectric properties of the produced copper oxide nanostructures for super capacitor applications. A novel symmetric super capacitor using CuO electrode was constructed with a two-electrode setup, and the cyclic voltammetry measurements for the same provide important insights into the electrochemical behavior of the system.

EXPERIMENTAL

Material and Methods

Cupric nitrate trihydrate [Cu $(NO_3)_2 \cdot 3H_2O$] (Hi media 99.5% purity) was used as the precursor salt. CTAB (Cetyltrimethyl ammonium bromide), PVP k_{30}(Poly Vinyl Pyrrolidone) [Hi media] and Igepal - 210 [Sigma Aldrich] were the surfactants used for the synthesis. Sodium hydroxide pellets [NaOH] (Nice chemicals) was used as a reductant. An analytical reagent-grade chemical without further purification was used for the synthesis.

Surfactant-Assisted Wet Chemical Method

Solutions of 0.1M cupric nitrate and 0.2 M NaOH were prepared individually using de-ionised water. A freshly prepared sodium hydroxide solution was incrementally added drop wise to the cupric nitrate solution with continuous stirring until the pH of the base solution reached a simultaneously a blue colour precipitation was produced and subsequently transformed into black colour. A suction funnel was then used to wash the precipitate repeatedly with distilled water and ethanol. Washed samples were dried at room temperature for 24 hrs. Then it was kept in an oven at 120° C for 10 hours and labeled as NS (w). The same procedure was followed to synthesis surfactant-assisted samples as well, except for the addition of a stoichiometric amount of surfactant with copper nitrate solution, along with the continuous stirring at tepid temperature. 0.005 M of PVP, 0.001M and 0.01M of CTAB concentrations were preferred in this study for the comparative analysis, which were labelled as PVP (0.005), CT (0.001) and CT (0.01).

Solid-State Reaction Method

0.01 M of cupric nitrate and 0.2 M of sodium hydroxide pellets were ground using the agate and mortar till resulting a blue color pasty copper hydroxide resulted. Ethanol and de-ionised water were used to wash the as-prepared copper hydroxide thoroughly before placing the same in a furnace at 300° °C for 5 hrs. The heat treatments turn the CuO material black in color and are labeled as NS(s). The same procedure was followed to synthesis surfactant-assisted samples as well, except that the cupric nitrate was ground initially with a stoichiometric amount of 0.1 M of Igepal as surfactant. The copper hydroxide was then washed thoroughly with ethanol, followed by de-ionised water and labeled as IG (0.1).

Electrode Preparation

The electrode was prepared from a slurry mixture composed of 80wt% copper oxide, 15wt% carbon black (Alfa Aesar) and 5wt% poly-vinylidene fluoride (PVDF) as binder in N-methyl-2-pyrrolidone (NMP) as solvent. The mixed slurry was coated onto a cleaned copper foil substrate based on the "doctor blade technique". Coated foil was dried at 120°C for 12 hours under vacuum for the complete removal of the solvent, and then the foil was pressed under a roller press. The coated electrode specimen was cut into squares (1cm x 1cm dimension) such that the part with some empty foil.

RESULTS AND DISCUSSION

XRD Analysis

The XRD patterns of the copper oxide nanostructures synthesised in pure form and with surfactant assistance are comparatively depicted in Fig.-1. Prominent and wide peaks are observed in the XRD patterns of the materials, indicating their nano crystalline characteristics. All the peaks attributed to the monoclinic crystal system are in good agreement with JCPDS card number 80-1916.

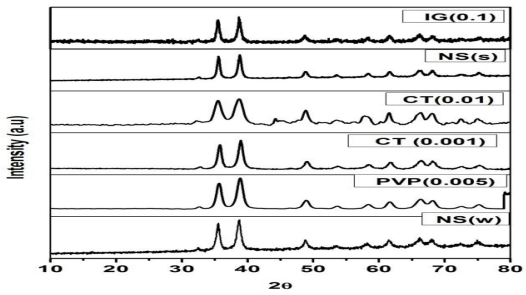

Fig.-1: XRD Pattern of the Synthesised CuO Nanostructures

The crystallite size of the materials was calculated using Scherer's formula.

$$D = \frac{0.9\lambda}{\beta cos\theta}$$

Where D is the crystallite size, λ is the Wavelength used, β is the Full width at half maximum, and θ is the diffraction angle. The crystallite sizes determined using Scherer's formula are 21, 36, 33, 18, 44, and 25 nanometers for the samples NS (w), PVP (0.005), CT (0.001), CT (0.1), NS (s) and IG (0.1), respectively. Among the samples synthesised using the wet chemical method, the crystallite size for CT (0.01) is observed to be minimal. The crystallite sizes of the CT (0.001) and PVP (0.005) samples are greater than those of the sample produced without surfactant (NS(w)). The augmentation in crystallite size may result from the thermal treatment aimed at dissolving the surfactants.

Williamson – Hall (W-H) Plot

The crystallinity size and strain of the synthesised CuO nanoparticles are determined from the XRD data using the Williamson–Hall (W-H) plot method. The micro-strains in the CuO nanoparticles are caused by the incoherent diffraction domains. Peak broadening appears in the experimental data of the XRD pattern, where the broad peaks signify the nanoparticles' smaller crystal size. Let the equation relate the micro-strain $\beta\varepsilon$, crystallite size β_D, and peak broadening β_T. Total broadening is equal to the sum of the strain and crystallite size.

$\beta_T = \beta_\varepsilon + \beta_D$

The micro–strain can be calculated by using the relation.

$\beta_\varepsilon = 4\varepsilon \tan\theta$

From the Scherrer equation,

$\beta_D = K\lambda / D \cos\theta$

$\beta_T = 4\varepsilon \tan\theta + K\lambda / D \cos\theta$

Simplifying and get

$\beta_T \cos\theta = 4\varepsilon \tan\theta + K\lambda / D \cos\theta$

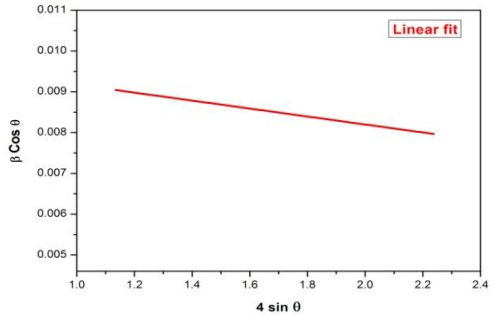

Fig.-2: Williamson–Hall (W-H) plotCuO Nanostructures

A straight-line equation where the Y-intercept (Kλ/D) is used to calculate the crystalline size, and the slope of the linear fit is ε (strain). Plotting the graph between 4 sin θ and the Y-axis, β_T cos θ, allows one to study the W-H plot. The nanocrystal line size and micro strain was calculated from the graph shown in Fig 2. The value of micro–strain is 9.76 x10^{-4} and crystalline size is 21 nm.

SEM Analysis

The Carl ZEISS – EVO 18 Scanning electron microscope was used to study the morphological information of the synthesised sample. The SEM imaging is performed to identify the morphology of copper oxide in pure and with surfactant assistance samples for a magnification of 500nm. The morphology of the samples displayed a strong correlation with the surfactant assistance and preparation method, indicating evidence of structural moderation. Figure-3a. Shows that the copper oxide in pure form, without the assistance of surfactant, prepared through the wet chemical method, has a flake structure. It is evident from SEM images presented in Fig.-3b, 3c and 3d that the assistance of surfactants PVP and CT in copper oxide samples prepared via the wet chemical method impacts the structural change in leaves and flower pattern. In contrast, the morphological structures in Fig.-3e and 3f of the copper oxide in pure form without the assistance of surfactant, prepared through the solid-state reaction method, have a particle structure, and the morphology is changed to a sponge-like structure as the above-said sample is assisted with IG surfactant. The evidence of porous structure in all the images might be the result of the heat treatment involved in the synthesis process.

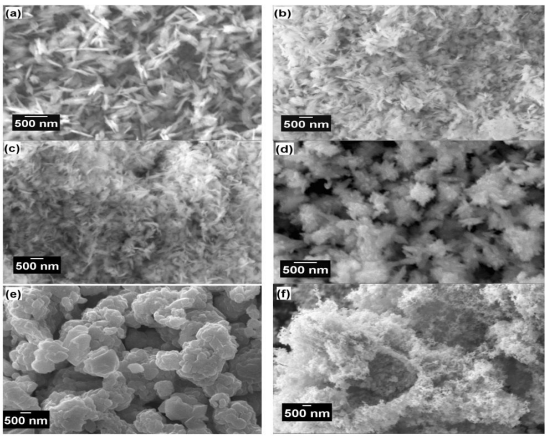

Fig.-3: SEM Pictures of the CuO Nanostructures Synthesised with different Synthesis Routes and Surfactant Assistance, (a) NS(w), (b) PVP (0.005), (c) CT (0.001), (d) CT (0.1), (e) NS(s) and (f) IG (0.1).

Dielectric Properties

Material's dielectric behaviour can be described by the complex permittivity is given by,

$$\varepsilon^* = \varepsilon\omega\ (\omega) - j\ \varepsilon\omega\ (\omega) = j/\omega C_0 Z^*$$

Where $\varepsilon\omega(\omega)$ and $\varepsilon\omega\ (\omega)$ are the real (dielectric constant) and imaginary part (dielectric loss) of the complex permittivity. Dielectric constant is the ability of the material to store charge in the presence of an electric field, while dielectric loss is a measure of energy losses to move ions when the polarity of the electric field reverses rapidly. The real part of the dielectric constant is calculated by the formula. $\epsilon' = \frac{cd}{A\epsilon_0}$, Where 'c' is the capacitance, 'd' is the thickness of the pellet, 'A' is the surface area of the pellet and 'ε_0' is the absolute permittivity (8.854 x 10^{-12} F/m). The imaginary part of the dielectric constant is expressed as $\epsilon'' = \epsilon' tan\delta$ And 'tan δ' is the dielectric loss factor.

Figure-4 (a-f) shows the variation of εw with frequency at different temperatures for the synthesized CuO nanostructures synthesized by wet chemical method and solid-state reaction method with the assistance of surfactant. It is observed that the magnitude of the dielectric constant is quite high at lower frequencies of applied ac field and then drops with increasing frequency, and eventually it achieves constant low value at

higher frequency. This can be explained by multiple low-frequency polarisation mechanisms. In the low frequency range, dipolar and space charge processes predominate, where as electronic and ionic polarisations are active in the high frequency range. At low frequencies, the charges associated with defects can be more easily rearranged, causing defects nearer to the positive end of the applied field to acquire a negative charge, while those closer to the negative end of the field become positively charged. As the frequency rises, the dipole moments cannot adjust quickly enough to stay aligned with the external field, resulting in a decrease in total polarizability. Consequently, the dielectric constant decreases and subsequently becomes unaffected by the frequency of the applied field. From Fig.-4, it can also be observed that the dielectric constant of all the materials rises with an increase in temperature.

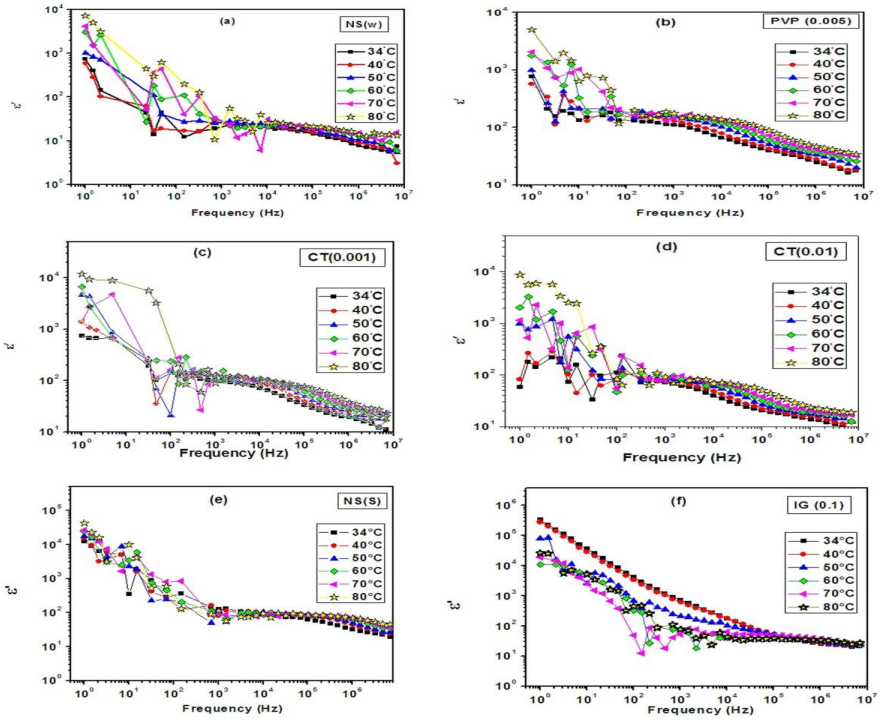

Fig.-4: Variation of Dielectric Constant of the CuO Nanostructures with Frequency at different temperatures

As the temperature rises, it provides energy to the material, allowing the dipoles to orient, thereby enhancing orientation polarisation and subsequently increasing the dielectric constant. Furthermore, the temperature rise generates electron-hole pairs, creating an additional dipole moment. This also contributes to the increase in the dielectric constant of the materials as temperature increases. Figure-4(a-d) illustrates the dielectric properties of CuO nanoparticles in both pure and surfactant-assisted samples with various concentrations, synthesised via the wet chemical approach, exhibiting a comparable pattern. The pattern comprises three regions: (i) a sharply decreasing region at low frequencies of the applied field, (ii) a frequency-independent region in the middle, and (iii) a slowly decreasing region at higher frequencies. Figures-4(a-d) illustrates that the frequency at which the transition between the middle region and the slowly decreasing region occurs due to the temperature increase. The CuO nanomaterial, synthesised via the solid-state reaction approach (NS (w)) and with the aid of surfactant IG (0.1), as illustrated in Fig.-4(e) and 4(f), exhibits only two distinct regions, excluding the intermediate region. This demonstrates that the samples' dielectric behaviour varies according to their morphology and synthesis technique. The dielectric constant values for CuO materials synthesised via the solid-state reaction technique also vary. PVP (0.005) sample has an ε′ value in the same range as NS(w), which has the highest dielectric constant at low frequency and high temperature in the order of 103. The IG (0.1) sample achieves the ε′ value in the order of 10^5, whereas the maximum values for the CT (0.001), CT (0.01), and NS(s) are in the order of 10^4. The presence of microscopic amounts of Cu^{3+} plays a vital role. Holes hop between Cu^{2+} and Cu^{3+}, governing the conduction mechanism of the CuO materials. He also discussed the grains acting as semiconductors

due to the presence of Cu^{3+}, and the grain boundaries acting as insulating walls due to the absence of Cu^{3+}. The array of these grains and grain boundaries is a reason for the high dielectric permittivity of the material. Moreover, the concentration of Cu^{3+} depends on the heat treatment during the synthesis of materials. According to the current investigation, NS(s) and IG (0.1) synthesised at a higher temperature using the solid-state reaction approach might have a larger concentration of Cu^{3+} and, thus, more permittivity than other samples. CuO, a lead-free high-dielectric substance, has a special feature that makes it a potentially useful material for a super capacitor electrode. Figure-5(a-f) illustrates the dielectric loss of the synthetic materials. The dielectric constant (ε′) and fluctuations in dielectric loss (ε_Θ) exhibit a comparable trend. ε increases with elevated temperature and decreases linearly with increased frequency. This behaviour indicates that the materials demonstrate increased polarisation effects at elevated temperatures, whilst the impact of frequency results in a diminished capacity to respond to the electric field. Thus, these findings demonstrate that meticulous attention to temperature and frequency is crucial for enhancing the efficacy of synthetic dielectric materials across many applications. The dominant mechanism responsible for the increased loss at high temperatures is the effect of DC conductivity. We observed very high dielectric loss for the material under investigation. To measure this, we created a capacitor structure using stainless steel electrodes clamped to the material with crocodile clips. However, the resulting high loss could be an artefact of contact resistance or other conduction issues at the electrode-material interface.

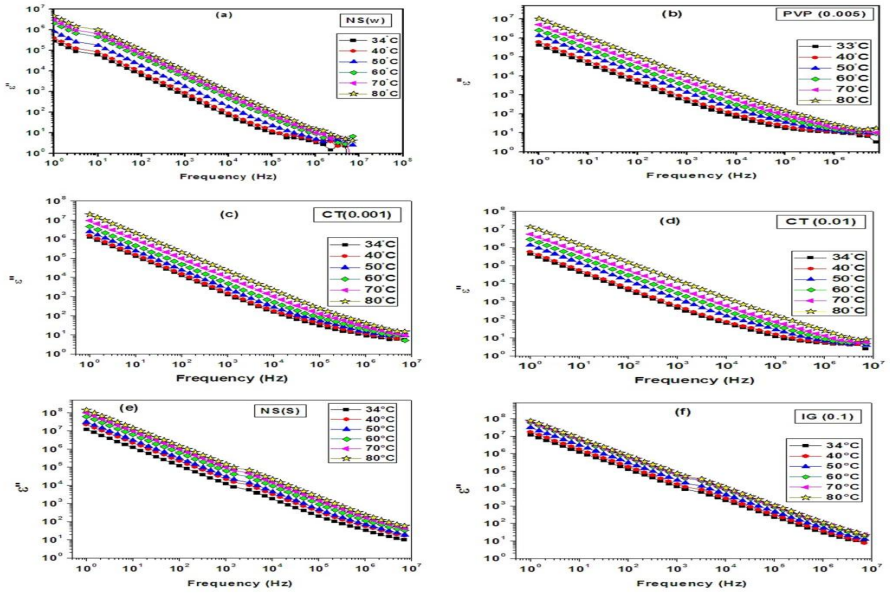

Fig.-5: Variation of Dielectric Loss of the CuO Nanostructures with Frequency at different Temperatures

Electrochemical Property Analysis

Previous studies have investigated the electrochemical performance of CuO nanostructures primarily using three-electrode configurations; this work presents, for the first time, electrochemical characterisation using a two-electrode beaker cell with a symmetrical configuration. They demonstrated that capacitance values obtained from three-electrode cells are significantly higher than those of packaged super capacitors, whereas two-electrode measurements provide more accurate results. The previously reported two-electrode asymmetric super capacitors based on CuO and AC electrodes. In our experiments, the prepared electrodes were positioned face-to-face with a small gap within a beaker containing 1M Na_2SO_4 electrolyte, ensuring full immersion of the coated area. Cyclic voltammetry (CV) was performed within a potential window of 0 to 0.5 V.

Cyclic Voltammetry Studies

Cyclic voltammetry (CV) was performed on the CuO nanostructure electrodes at scan rates of 5, 10, 25, 50, 75, and 100 mV/s (Fig.-6a- f). The resulting CV curves displayed a quasi-rectangular shape without

distinct redox peaks. This is somewhat atypical for CuO, as many reports show CV curves with clear redox features, indicating a pseudo-capacitive charge storage mechanism. The absence of pronounced redox peaks in our study suggests that pseudo-capacitance plays a less significant role. This difference may be attributed to the symmetric super capacitor configuration employed, where only a small potential difference exists between the identical electrodes. This limited potential may allow for ion separation in the electrolyte but not the intercalation of ions into the CuO. Notably, the shape of the CV curves remained relatively consistent across varying scan rates, highlighting the good electronic conductivity within the CuO nanostructures. The linear increase in voltammetric current with increasing scan rate further confirms the capacitive nature of the device. The measured currents were normalised by the mass of a single electrode.

The CV curve of the IG (0.1) sample exhibits redox peaks, even at high scan rates, suggesting additional redox reactions compared to the other samples. This may be attributed to the sponge-like morphology of IG (0.1), which facilitates electrolyte ion access even at small potential differences. The specific capacitance, C_s of a single Cu electrode was determined using the formula $C_s = \frac{\int IVdV}{vs}$. In this equation, 'I' represents the average current derived from the integrated CV curve using EC Lab software, 'V' is the potential window, and 's' is the scan rate. Recognising the impact of a two-electrode configuration on capacitance measurements, the cell capacitance c_{cell} was calculated, as-

$$c_{cell} = \frac{c_s}{4}$$

This correction accounts for the combined contributions of both electrodes and the fact that a two-electrode capacitor has half the capacitance but double the weight of a single electrode. The resulting specific capacitance values for individual electrodes and the complete cell are summarised in Table-1 for all CuO nanostructure samples.

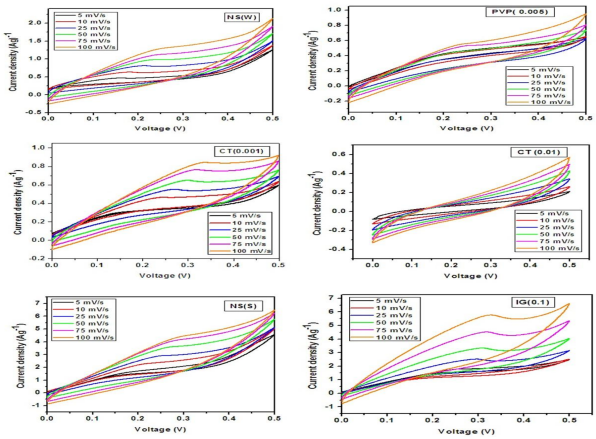

Fig.-6: Cyclic Voltammetry of the CuO Nanostructures Synthesised with different Synthesis Routes and Surfactant Assistance

Table-1: Specific Capacitance Values of the Synthesized CuO Nanostructures

Scan rate mVs^{-1}	Specific capacitance (F/g)											
	NS(w)		CT (0.001)		CT(0.01)		PVP (0.005)		NS(s)		IG(0.1)	
	S_e	S_{cell}	S_e	S_{cell}	S_e	S_{cell}	S_e	S_{cell}	S_e	S_{cell}	S_e	S_{cell}
5	208	51	132	33	20	5	152	38	747	186	572	143
10	118	29	73	18	10	2.5	72	18	414	104	249	62
25	51	13	30	8	4.5	1.1	24	6	171	43	135	33
50	28	7	16	4	2.5	0.63	13	3	94	24	82	20
75	20	5	11	3	1.8	0.47	9	2.3	66	17	69	17
100	17	4	9	2	1.5	0.39	7.5	1.9	52	13	62	16

Among the synthesised CuO nanostructures, sample NS(s) displayed the highest specific capacitance. The resulting cell capacitance. C_{cell} for NS(s) reached 186 F/g, demonstrating its promising capacitive performance relative to other CuO-based materials. Importantly, even the other CuO samples exhibited competitive specific capacitance values that are higher than those reported in studies using three-electrode configurations, further highlighting the potential benefits of our two-electrode approach.

CONCLUSION

Copper oxide nanostructures with varying morphologies were synthesised using both surfactant-assisted wet chemical and solid-state reaction methods. The synthesis method and the addition of surfactants significantly influence the morphology, dielectric properties, and electrochemical behaviour of the resulting CuO nanostructures. The prominent dielectric behaviour of the synthesised materials was examined. A symmetric super capacitor, employing a two-electrode configuration with CuO electrodes, was constructed and characterised via CV measurements. A high specific capacitance of 747 F/g was achieved for a single electrode, and 186 F/g for the entire cell, using CuO nanostructures synthesised via the solid-state reaction method.

ACKNOWLEDGMENTS

The authors would like to thank Dr. Akhila Kumar Sagu, CSIR principal scientist, and Dr. Magesh Kumar SPO, CSIR Chennai Tharamani Complex, Chennai, for their constant support and encouragement. The authors are very grateful for the constant support provided by Rev. Dr Pavulraj Michael S.J., Rector, Rev. Dr S. Mariadoss S.J, the principal of St. Joseph's College (Autonomous) Tirchirappalli, and Rev. Dr P. Arockiasamy Xavier S.J, the secretary of St. Joseph's College (Autonomous) Tirchirappalli.

CONFLICT OF INTERESTS

The authors have no conflicts of interest to declare. All co-authors have agreed with the contents of the manuscript, and there is no financial interest to report.

AUTHOR CONTRIBUTIONS

The present work is related to *SDG-7: Affordable and Clean Energy*. All the authors contributed significantly to this manuscript, participated in reviewing/editing and approved the final draft for publication. The research profile of the authors can be verified from their ORCID ids, given below:

M.Sappani Muthu http://orchd.org/0000-0003-3882-2547
J. Judes http://orchd.org/ 0000-0002-6546-8398
S. Arul Ravi http://orchd.org/0000-0002-5323-9088
M. Ambrose Rajkumar http://orchd.org/0000-0003-1805-8123

Cite this article as: M. Sappani Muthu *et al.*, *Rasayan J. Chem.*, 19(1), 114-122(2026), https://doi.org/10.31788/RJC.2026.1919498

REFERENCES

1. M.S. Muthu, P. Ajith, J. Agnes, *Journal of Material Science: Material Electronics,* **34,** 1766(2023), https://doi.org/10.1007/s10854-023-11085-3
2. M.S. Muthu, M.A, Raj Kumar, P. Ajith, *Journal of Material Science: Material Electronics,* **36,** 785 (2025), https://doi.org/10.1007/s10854-025-14644-y
3. A.R. Nair, T.V. Balakrishnan, R.N. Bulakhe, J.M. Kim, S.N. Sawant, and A.D. Jagadale, *ACS Applied Energy Materials*, **7(22),** 10346 (2024), https://doi.org/10.1021/acsaem.4c01749
4. B.T. Vetrikarasan, A.R. Nair, *Journal of Energy Storage*, **94,** 112457(2024), https://doi.org/10.1016/j.est.2024.112457

5. Y. Shao, M.F. El-Kady, J. Sun, *Chemical Reviews*, **118(18),** 9233(2018), https://doi.org/10.1021/acs.chemrev.8b00252
6. G. M . Kanaginahal, R.S. Mahale, V.K Shamanth, *Nano Hybrids and Composites*, **39,** 17(2023), https://doi.org/10.4028/p-si6964
7. N. Wu, X. Bai, D. Pan, B. Dong, R. Wei, N. Naik, *Advanced Materials Interfaces*, **8(1),** 2001710 (2021), https://doi.org/10.1002/admi.202001710'
8. S. Chen, G. Meng, B. Kong, B. Xiao, Z. Wang, *Chemical Engineering Journal*, **387,** 123662 (2020), https://doi.org/10.1016/j.cej.2019.123662
9. S. Pratyusha, P. Latha,M.R. Reddy and M. Nakka, *Journal of Molecular Structure*, **1315,** 138759 (2024), https://doi.org/10.1016/j.molstruc.2024.138759
10. M.M Abdelhamied, A. Atta, B. M. Alotaibi, *Inorganic Chemistry Communications*, **157,** 111245 (2023), https://doi.org/10.1016/j.inoche.2023.111245
11. J. Qiu, Q. Gu, Y. Sha, Y. Huang, M. Zhang, and Z. Luo, *Journal of Applied Polymer Science*, **139(24),** 52367 (2022), https://doi.org/10.1002/app.52367
12. H.P.P.V. Shanmugasundram, E. Jayamani, and K.H. Soon, *Renewable and Sustainable Energy Reviews*, **157,** 112075 (2022), https://doi.org/10.1016/j.rser.2022.112075
13. J. Xie, Z. Zhu, H. Tao, S. Zhou, Z. Liang, Z. Li, and J. Peng, *Journal of Coatings*, **10(7),** 698(2020), https://doi.org/10.3390/coatings10070698
14. D.Q. Tan, *Journal of Applied Polymer Science*, **137(33),** 49379(2020), https://doi.org/10.1002/app.49379
15. M. Yuan, B. Li, S. Zhang, R. Rajagopalan, and M.T. Lanagan, *ACS Applied Polymer Materials*, **2(3),** 1356 (2020), https://doi.org/10.1021/acsapm.9b01224
16. M.S. Muthu, P. Ajith, J. Agnes, M.S. Selvakumar, M. Presheth, and D.P. Anand, *Rasayan Journal of Chemistry*, **16(1)** (2023), http://doi.org/10.31788/RJC.2023.1618190
17. A. Sudhakaran, A. Sudhakaran, and E. Sivasenthil, *Journal of Electronic Materials*, **53(8),** 4622 (2024), https://doi.org/10.1007/s11664-024-11197-4

[RJC-9498/2025]